

Higher harmonics imaging in tapping-mode atomic-force microscopy

Robert W. Stark^{a)} and Wolfgang M. Heckl

Ludwig-Maximilians-Universität München, Sektion Kristallographie, Theresienstrasse 41,
80333 Munich, Germany

(Received 27 June 2003; accepted 14 September 2003)

In tapping-mode atomic-force microscopy usually amplitude and phase of the cantilever motion are acquired. These signals are related to the fundamental oscillation frequency neglecting information at higher frequencies. However, the nonlinear contact between tip and sample induces higher frequency vibrations that are harmonics of the fundamental. In order to recover the available information the full tip motion has to be analyzed. The higher harmonics can be employed for image formation. A setup that consists of two independently operated lock-in amplifiers is used to detect higher harmonics in the dynamic atomic-force microscopy signal. Higher harmonic imaging proves to be useful to monitor the imaging conditions in tapping mode and can be applied for nanoscale imaging with a material contrast. © 2003 American Institute of Physics.

[DOI: 10.1063/1.1626008]

I. INTRODUCTION

In the standard setup of tapping-mode atomic-force microscopy (TMAFM) the cantilever is resonantly excited to an oscillation amplitude of a few nanometers. The mechanical interaction between tip and sample constrains the oscillation amplitude, which is used for feedback in order to measure the sample topography. The nonlinear tip sample interaction gives rise to a complicated dynamics.¹⁻³ The existence of different oscillatory states in tapping mode and noncontact AFM as well as their stability were investigated with numerical simulations.⁴ Despite the mathematical difficulties due to the nonlinearities TMAFM is widely used for topographic imaging.

An important application of TMAFM is the determination of surface properties by measurement of the phase lag between the driving signal and the cantilever response.⁵ For this purpose the average deflection, amplitude, and phase of the cantilever motion are conventionally recorded in TMAFM. This corresponds to the first two Fourier coefficients of the cantilever motion, i.e., the constant and the first order coefficient. Thus only data in a first order approximation are acquired and the higher degree information is lost. However, it is exactly in the higher harmonics of the signal, where the information about the nonlinear tip sample interaction is encoded.⁶⁻¹⁰ The full analysis of the entire spectral information allows one to recover the time resolved interaction force between tip and sample.¹¹

In the following we demonstrate that the higher harmonic signals can be used to discriminate between different materials and to determine the operating conditions of the tapping mode AFM.

II. THEORETICAL BACKGROUND

In this section, a brief outline of the theoretical background will be given. For a theoretical description of dy-

namic AFM one has to consider that the micromechanical cantilever is a dynamic system that has many degrees of oscillatory freedoms (eigenmodes). Anharmonic external forces due to nonlinear interactions introduce multiples of the base frequency (higher harmonics) that excite the dynamic system at higher frequencies. The typical thickness of an AFM cantilever is in the order of a few microns, the length is in the order of 100 μm . The oscillation amplitude in TMAFM is usually adjusted to a few nanometers, typically in the range from 5 to 100 nm. Thus the vibrating cantilever can be considered as a linear system. The equation of motion of a rectangular cantilever can be approximated by the one-dimensional Euler-Bernoulli equation for the time dependent transverse displacement of the centerline $v(x,t)$ from the neutral position¹²

$$EI \frac{\partial^4}{\partial x^4} \left(v(x,t) + a_1 \frac{\partial v(x,t)}{\partial t} \right) + m(x) \frac{\partial^2 v(x,t)}{\partial t^2} + a_0 m(x) \frac{\partial v(x,t)}{\partial t} = f(x,t). \quad (1)$$

The mass density of the material $m(x)$, the moment of inertia $I(x)$, and the Young's modulus $E(x)$ are assumed to be constant. Damping is described by two parameters: a mass proportional damping parameter a_0 and a stiffness proportional damping parameter a_1 . Thus the damping of the i th mode is $\gamma_i = a_0/2\omega_i + a_1\omega_i/2$. This choice of damping provides a realistic model of the modal damping and allows one to transform Eq. (1) into normal coordinates. The eigenfunctions $\varphi_n(x)$ of the undamped system are used in order to obtain decoupled ordinary differential equations. For arbitrary cantilever geometries the eigenmodes are obtained by a straightforward finite element analysis.^{13,14}

The tip-sample interaction introduces a nonlinearity into the system. Close to a surface the van der Waals forces lead to an attractive interaction force ($z - z_s \geq a_0$), where z and z_s are the tip deflection and the position of the sample, respectively. The mechanical contact at $z - z_s < a_0$ leads to a repul-

^{a)}Author to whom correspondence should be addressed; electronic mail: stark@nanomanipulation.de

sive interaction force. Systems without energy dissipation in the tip-sample contact can be modeled using a Derjaguin-Müller-Toporov (DMT) model¹⁵ leading to

$$f_{\text{ts}}(z) = \begin{cases} -HR/[6(z-z_s)^2], & z-z_s \geq a_0 \\ -HR/6a_0^2 + \frac{4}{3}E^* \sqrt{R}(a_0-z+z_s)^{3/2}, & z-z_s < a_0 \end{cases} \quad (2)$$

Here, H is the Hamaker constant and R the tip radius. The parameter a_0 is an interatomic distance that usually is introduced to avoid numerical divergence of F_{ts} .¹⁶ The effective contact stiffness is given by $E^* = [(1-\nu_t^2)/E_t + (1-\nu_s^2)/E_s]^{-1}$, where E_t and E_s are the respective elastic moduli and ν_t and ν_s the Poisson ratios of tip and sample.

The nonlinearity introduced by Eq. (2) gives rise to the generation of higher harmonics in the AFM signal. Solving Eq. (1) or the equivalent finite element problem with the appropriate boundary conditions for the clamped end together with Eq. (2), the time dependent force of the vibro-impacting system can be obtained.^{6,9,10} For steady-state conditions the resulting interaction force can be expanded in a Fourier series. The individual Fourier coefficients depend on the exact shape of the interaction potential in Eq. (2). The shape of the force pulse depends on the local material properties of the specimen, e.g., H and E^* in the simple model of Eq. (2). This allows one to distinguish surface areas with different material properties already by acquisition of a single higher harmonic. Due to the resonance behavior of the cantilever the higher order harmonics in the AFM signal are sufficiently large to be detected by a lock-in technique.

III. EXPERIMENT

For the detection of the anharmonic signals, a commercial atomic force microscope (TopoMetrix Explorer, Veeco/TM Microscopes, Sunnyvale, CA) was modified. In this system the bandwidth was limited to $f_c \approx 50$ kHz by the photodiode preamplifier. Thus signals are damped by a factor of 10 at $f = 500$ kHz due to the low pass characteristics of the electronic circuit. The signals were demodulated by a lock-in amplifier (EG&G 5302, EG&G Inc., Princeton) with a time constant of $100 \mu\text{s}$. The lock-in amplifier output (x, y) was transformed into polar coordinates (r, ϕ) by a dedicated converter electronics. The signal amplitude r was used for AFM feedback. An external function generator (DS 345, Stanford Research) was used for the generation of the AFM driving signal. A second lock-in amplifier (SR 844, Stanford Research Systems) was used for the detection of the higher harmonic signals (Fig. 1). The reference signal was generated with a second function generator of the same type. To maintain phase stability both function generators were coupled by a 10 MHz frequency standard. This separated detection of the fundamental and the harmonic frequency assured that only higher harmonics of the AFM signal are detected avoiding possible generation of harmonics due to the signal mixing in the lock-in amplifier.

In order to obtain higher order harmonics within the limited bandwidth of the photodiode preamplifier a cantilever with a low resonant frequency was employed (Silicon cantilever NSCS 11, lever A, v-shaped, nominal spring constant

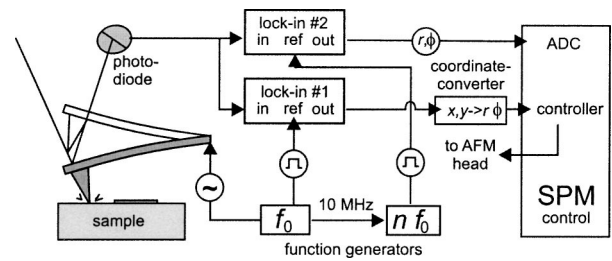


FIG. 1. Experimental setup for the detection of anharmonic signals. A commercial AFM is equipped with a second lock-in amplifier for the detection of anharmonic signals.

3.0 N/m, Mikromasch, Tallinn, Estonia). The resonant frequency of the transverse modes were $f_1 = 52.2$ kHz, $f_3 = 264.5$ kHz, and $f_5 = 417.6$ kHz. The eigenfrequencies f_2 and f_4 belong to torsional vibration modes of the cantilever that do not contribute the force signal. The actual spring constant $c = 3.1$ N/m was determined by the analysis of the thermomechanical noise of the cantilever in combination with a finite element analysis.¹⁷

IV. RESULTS AND DISCUSSION

To demonstrate that higher harmonic imaging allows one to clearly differentiate between distinct materials a shadow evaporation mask of a 4-nm-thick platinum carbon (Pt-C) layer on a fused silica coverslip was imaged in tapping-mode AFM. The cantilever was excited at its fundamental resonance frequency of $f_1 = 52.2$ kHz. The amplitude of the freely vibrating tip was set to $A_0 = 50$ nm, the set point was adjusted to an amplitude of 60% of the free amplitude. The topographical image and the control error (amplitude) image were acquired simultaneously together with one higher harmonic image. In order to compare the images of several harmonics, higher harmonic images were obtained consecutively. Figure 2 shows the topography (a), control error (b), and higher harmonics (c)–(e).

In the higher harmonic images in Figs. 2(c)–2(e) the material contrast between the Pt-C film and the glass sub-

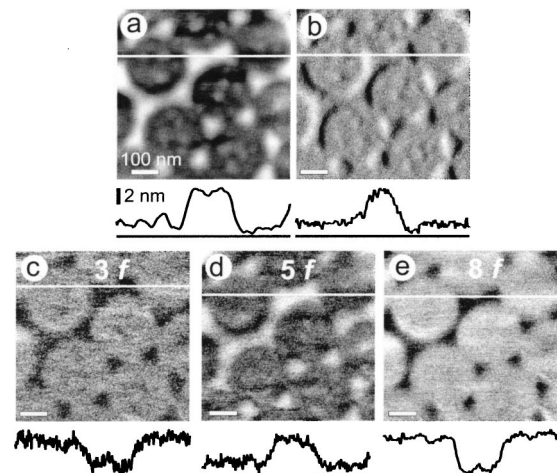


FIG. 2. (a) Topographic (b) control error, and (c)–(e) higher order harmonic images of a 4-nm-thick Pt-C test structure on a fused silica cover slip. The driving frequency was $f = 52.2$ kHz, the detection frequencies were (c) $3f = 156.6$ kHz, (d) $5f = 261.0$ kHz, and (e) $8f = 417.6$ kHz.

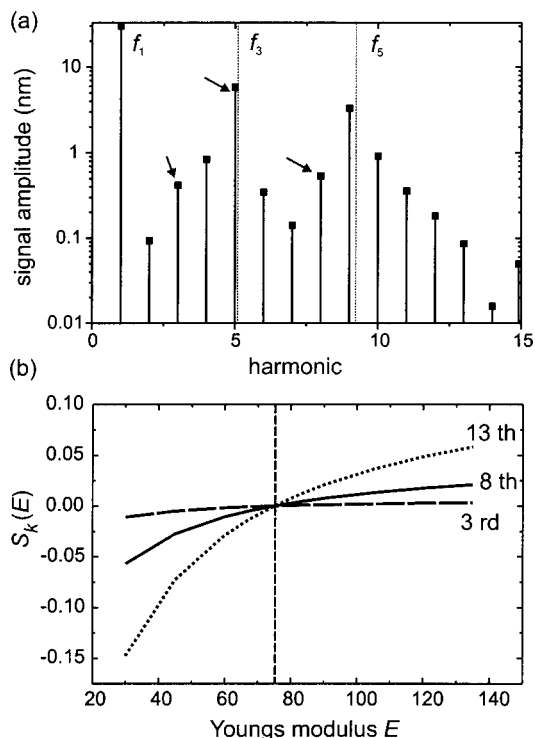


FIG. 3. (a) Calculated amplitude of the harmonics of the cantilever response to the periodic interaction with the glass substrate. The transverse resonance frequencies are indicated by the dashed lines. The arrows indicate the third, fifth, and eighth harmonic. (b) Calculated sensitivity of the harmonic amplitudes as indicated to variations of the Young's modulus. The vertical dashed line gives the Young's modulus of the glass surface that was used as a reference.

strate was prominent. In the higher harmonic images at $3f_1$ and $8f_1$ [(c) and (e)] the Pt-C layer appeared darker as compared to the glass substrate. However, a contrast reversal at $5f_1$ in Fig. 2(d) as compared to the harmonics in Figs. 2(c) and 2(e) was observed. From the cross sectional analysis it can be seen that the signal-to-noise ratio of the higher order harmonic image at $8f_1$ was increased by an order of magnitude as compared to the image acquired at $3f_1$.

A numerical simulation of the steady state was carried out similar to the procedure described elsewhere.^{6,13} To account for the experimental situation the theoretical resonant frequencies were fit to the measured data. From this analysis the parameters for the decoupled eigenmodes were obtained and used for the numerical simulation of the tapping mode as described by Eqs. (1) and (2). Material parameters corresponding to a silicon tip that interacts with a fused silica surface were selected ($E_{\text{tip}}=129$ GPa, $\nu_{\text{tip}}=0.28$, $E_{\text{sample}}=75$ GPa, $\nu_s=0.17$). The Fourier coefficients of the time dependent interaction force between tip and sample were determined by fast Fourier transformation (FFT) of the steady state solution. Figure 3(a) gives the calculated anharmonic contributions in the photodiode signal as calculated for the glass substrate. The transverse resonant frequencies of the cantilever are indicated by the dashed lines. Figure 3(b) shows the sensitivity of the amplitude A_k of the k th harmonic,

$$S_k(E_{\text{sample}}) = A_k(E_{\text{sample}})/A_k(E_{\text{ref}}) - 1, \quad (3)$$

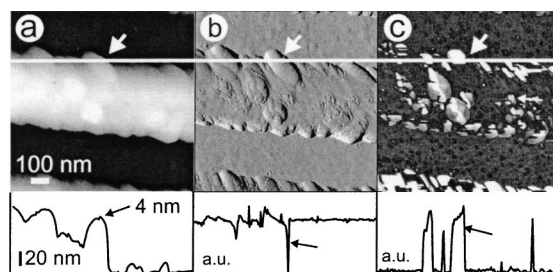


FIG. 4. Detail of a silicon test structure imaged in tapping mode (scan direction right to left). (a) Topography, (b) control error, and (c) eighth harmonic. The instabilities due to the bistable behavior of the system are difficult to be seen in the conventional images (a) and (b). However, in the harmonic image (c) a strong contrast prevails.

to variations of the Young's modulus of the sample E_{sample} . The respective calculated harmonic amplitude on the glass substrate ($E_{\text{ref}}=75$ GPa) was used as a reference.

From the simulation results it is clear that the signal-to-noise ratio of the higher modes depends on the frequency of the harmonic. Those harmonics that are close to a resonance frequency of the cantilever are enhanced and thus the ratio between the signal and the instrumental noise is improved. The fifth harmonic is close to a resonance which results in an increased signal amplitude as compared to the third harmonic. In the simulations the amplitude of the eighth harmonic is larger than the third harmonic. From the calculations the fifth and the eighth harmonic can be expected to offer a better signal-to-noise ratio as compared to the third. Experimentally, this can be seen in the cross sectional analysis in Figs. 2(c)–2(e). Additionally, the exact shape of the impact force (e.g., steepness and width) is encoded in the higher frequency Fourier components of the impact force.^{6,18} This means that there is an increased sensitivity to variations in the surface elasticity with increasing harmonic as can be seen in Fig. 3(b). The signal variations in the third harmonic for different elastic moduli are very small as compared to those in the eight and thirteenth harmonics. Although the simulations based on the simplifying model of the tip-sample contact in Eq. (2) explain the signal enhancement of the various modes they do not reproduce (data not shown) the contrast inversion observed in Fig. 2. Here, more sophisticated contact mechanical models are needed that account for the details of the tip-sample interaction like adhesion, capillary condensation, and viscous damping.

The practical use of higher harmonic signals for the determination of the imaging forces is illustrated in Fig. 4. A test specimen with a 100 nm high silicon oxide grating on a silicon substrate was imaged in tapping mode. The amplitude of the freely vibrating tip was set to $A_0=45$ nm, the amplitude set point was adjusted to 80% of the free amplitude. In the topography (a) and control error (b) image the structure of the grating could be obtained. However, in the higher harmonic image (c) a clear contrast prevailed. This can be explained as a consequence of the nonlinear tip-sample interaction in the imaging process that leads to the coexistence of two distinct stable states, the so-called high- and the low-amplitude state.⁴ A cross-sectional analysis reveals transitions of the dynamic system from the low-amplitude state in

the dark regions to the high-amplitude state in the bright regions. The sharp step in the higher harmonic image [arrow, Fig. 4 (c)] was accompanied by a sharp streak in the control error (b) and a small pseudotopographical step of about 4 nm (a). Since this step was induced by the transition from the low amplitude to the high amplitude state it does not reflect a real variation of the topography.

Thus the higher harmonic image can be used complementary to the phase image to assess the reliability of topographical images. Even with the limited bandwidth of the present setup it is possible to obtain images at higher harmonics. Since the higher harmonic image is directly related to the tip-sample forces it can be used as a monitor signal to optimize imaging conditions. Basically, large amplitudes in the higher harmonics indicate large repulsive tip-sample forces whereas small amplitudes are indicative of gentle imaging conditions. In order to obtain reliable topographic information also the variations in the higher harmonic signal should be minimized since this corresponds to a uniform imaging state.

Concluding, there is a twofold benefit in the acquisition of higher harmonic data. The higher harmonic image is useful to optimize the imaging conditions in tapping mode and allows one to differentiate qualitatively between dissimilar materials that are hardly distinguishable by conventional TMAFM. In order to obtain quantitative data on the mechanical characteristics of the specimen future developments will focus on an increased bandwidth of the detection system.

ACKNOWLEDGMENT

This work was supported by the Federal Ministry of Education and Research BMBF under Grant No. 03N8706.

- ¹N. Burnham, O. Behrend, F. Ouvevey, G. Gremaud, P. Gallo, D. Gourdon, E. Dupas, A. Kulik, H. Pollock, and G. Briggs, *Nanotechnology* **8**, 67 (1997).
- ²L. Nony, R. Boisgard, and J. P. Aimé, *J. Chem. Phys.* **111**, 1615 (1999).
- ³S. Lee, S. Howell, A. Raman, and R. Reifengerger, *Ultramicroscopy* **97**, 185 (2003).
- ⁴R. García and R. Perez, *Surf. Sci. Rep.* **47**, 197 (2002).
- ⁵S. Magonov, V. Elings, and M. Whangbo, *Surf. Sci.* **375**, L385 (1997).
- ⁶R. W. Stark and W. M. Heckl, *Surf. Sci.* **457**, 219 (2000).
- ⁷R. Hillenbrand, M. Stark, and R. Guckenberger, *Appl. Phys. Lett.* **76**, 3478 (2000).
- ⁸M. Stark, R. W. Stark, W. M. Heckl, and R. Guckenberger, *Appl. Phys. Lett.* **77**, 3293 (2000).
- ⁹O. Sahin and A. Atalar, *Appl. Phys. Lett.* **79**, 4455 (2001).
- ¹⁰T. R. Rodriguez and R. García, *Appl. Phys. Lett.* **80**, 1646 (2002).
- ¹¹M. Stark, R. W. Stark, W. M. Heckl, and R. Guckenberger, *Proc. Natl. Acad. Sci. U.S.A.* **99**, 8473 (2002).
- ¹²R. W. Clough and J. Penzien, *Dynamics of Structures* (McGraw-Hill, Singapore, 1993).
- ¹³R. W. Stark, T. Drobek, and W. M. Heckl, *Appl. Phys. Lett.* **74**, 3296 (1999).
- ¹⁴M. R. Hatch, *Vibration Simulation Using MATLAB and Ansys* (Chapman and Hall/CRC, London, 2000).
- ¹⁵B. V. Derjaguin, V. M. Muller, and P. Toporov Yu, *J. Colloid Interface Sci.* **53**, 314 (1975).
- ¹⁶R. García and A. San Paulo, *Phys. Rev. B* **61**, R13381 (2000).
- ¹⁷R. W. Stark, T. Drobek, and W. M. Heckl, *Ultramicroscopy* **86**, 207 (2001).
- ¹⁸A. Balantekin and A. Atalar, *Phys. Rev. B* **67**, 193404 (2003).